Tigrine Zahia[1]
Faculty of Physics,
Thermodynamics and Energetic
Systems Laboratory,
University of Sciences and Technology Houari
Boumediène (USTHB),
B.P32 El Alia, Bab Ezzouar,
Algiers 16111, Algeria;
Unité de Développement des
Equipements Solaires,
UDES/Centre de Développement des Energies
Renouvelables, CDER,
Bou-Ismail, Tipaza 42415, Algeria
e-mail: phyzahia@yahoo.fr

Mokhtari Faiza
Faculty of Physics,
Thermodynamics and Energetic Systems
Laboratory,
University of Sciences and Technology Houari
Boumediène (USTHB),
B.P32 El Alia, Bab Ezzouar
Algiers 16111, Algeria
e-mail: faiza_mokhtari@yahoo.fr

Bouabdallah Ahcène
Faculty of Physics,
Thermodynamics and Energetic
Systems Laboratory,
University of Sciences and Technology Houari
Boumediène (USTHB),
B.P32 El Alia, Bab Ezzouar
Algiers 16111, Algeria
e-mail: abbouab2002@yahoo.fr

Merah AbdelKrim
Faculty of Physics,
Thermodynamics and Energetic Systems
Laboratory,
University of Sciences and Technology Houari
Boumediène (USTHB),
B.P32 El Alia, Bab Ezzouar
Algiers 16111, Algeria
e-mail: karim_merah@yahoo.fr

Kharicha Abdellah
Department of Metallurgy,
Montauniversität Leoben,
Franz-Josef-Str. 18,
Leoben A-8700, Austria
e-mail: abdellah.kharicha@unileoben.ac.at

Numerical Study of the Buoyancy Effect on Magnetohydrodynamic Three-Dimensional LiPb Flow in a Rectangular Duct

In this paper, the effect of transverse magnetic field on a laminar liquid lead lithium flow in an insulating rectangular duct is numerically solved with three-dimensional (3D) simulations. Cases with and without buoyancy force are examined. The stability of the buoyant flow is studied for different values of the Hartmann number from 0 to 120. We focus on the combined influence of the Hartmann number and buoyancy on flow field, flow structure in the vicinity of walls and its stability. Velocity and temperature distributions are presented for different magnetic field strengths. It is shown that the magnetic field damps the velocity and leads to flow stabilization in the core fluid and generates magnetohydrodynamic (MHD) boundary layers at the walls, which become the main source of instabilities. The buoyant force is responsible of the generation of vortices and enhances the velocities in the core region. It can act together with the MHD forces to intensify the flow near the Hartmann layers. Two critical Hartmann numbers ($Ha_{c1} = 63$, $Ha_{c2} = 120$) are found. Ha_{c1} is corresponding to the separation of two MHD regimes: the first one is characterized by a core flow maximum velocity, whereas the second regime is featured by a maximum layer velocity and a pronounced buoyancy effect. Ha_{c2} is a threshold value of electromagnetic force indicating the onset of MHD instability through the generation of small vortices close to the side layers. [DOI: 10.1115/1.4035636]

Keywords: magnetohydrodynamics, 17Li–83Pb, liquid metal, buoyancy effect, Hartmann number, MHD flow

Introduction

Magnetohydrodynamic (MHD) flow plays a key role in many industrial applications such as aerodynamics [1], crystal growth [2], thermonuclear fusion [3], and metallurgy [4]. Several works have been devoted to the analysis and control of liquid metal flow and heat transfer in these engineering applications in rectangular [5–8], circular [9–11], triangular [12,13], trapezoidal [14], variable cross section and curved ducts [15].

The MHD flows in rectangular ducts have been studied since the relevant paper of Hartmann [16] in 1937. He performed a symmetric theoretical study by describing the source of pressure losses coupled with the fringing magnetic field and the formation of axial current loops. He has conducted the first experimental study with mercury inside different duct configurations in a homogeneous magnetic field. Later, Shercliff [17] studied experimentally and theoretically the MHD flow at high Hartmann number in pipes with insulating walls to analyze the boundary layers on the walls parallel to the field. He revealed that the axial currents effect favors the "M-shape" velocity profile and the associated vorticity.

[1]Corresponding author.

Contributed by the Fluids Engineering Division of ASME for publication in the Journal of Fluids Engineering. Manuscript received July 8, 2016; final manuscript received December 18, 2016; published online April 5, 2017. Assoc. Editor: Shizhi Qian.

In fact, two different types of flow boundary layers are present in the duct when the magnetic field is perpendicular to the flow direction. These layers are Hartmann layers that are formed at walls normal to the applied magnetic field and side layers are developed at walls parallel to B. Hartmann and side layers development are the main features in MHD liquid metal flow in a rectangular duct. They give a local distribution of the velocity field near the walls region. By definition, the boundary layer thickness of Hartmann (δ_{Ha}) and side layers (δ_{side}), is the distance across a boundary layer from the wall to a point where the flow velocity has essentially reached the mean velocity $V_0(V(Y) = 0.99V_0)$. A theoretical analysis of conducting liquid laminar motion in a rectangular duct with conducting parallel and insulating perpendicular walls to the transverse field has been performed by Hunt [18,19]. He has found the solution for high Hartmann numbers by analyzing the boundary layers on the walls and concluded that the magnetic field may have a destabilizing influence on the flow.

Numerous studies have been devoted to the numerical modeling [20–24] of the MHD flow in different cross section configurations and the phenomena of magneto-convection were found to include a diversity of nonlinear effects as instability bifurcations, symmetry breaking, and laminar-turbulent transition. Convective heat transfer behavior of steady state laminar liquid lithium flow in a horizontal circular pipe was examined theoretically and numerically by Recebli et al. [22] for two different cooling and heating conditions with constant wall temperature under the effect of a perpendicularly applied magnetic field.

Smolentsev et al. [23] reviewed different studies that treated instabilities and transitions in MHD flows in liquid metal blanket for fusion applications. They have shown that possible transitions affect the stability of Hartmann and side layers at lower Reynolds numbers associated with high velocity near-wall jets. The MHD mixed convection flow in a vertical insulating square duct under the effect of strong transverse magnetic field has been carried out by Chutia and Deka [24]. They observed that both buoyancy and Lorentz forces affect considerably the mixed convection.

At this time, there are a few studies about analytical solution of the MHD flow. Recent work was presented by Bluck and Wolfendale [25] about an analytical solution to the laminar flow of an electrically conducting fluid in an array of partially conducting ducts subjected to an applied magnetic field. These solutions provide an understanding of the physics of such flows and an important benchmarking and validation data for computational MHD. They have shown the effect of arbitrary walls thickness on the flow by demonstrating the limitations of the thin-wall approximation developed by Hunt. They also have found that there is an important modification of pressure drop and velocity profile when wall thickness is increased.

The numerical simulation of MHD flows and their heat transfer in duct is very important to understand the complex physics of liquid metal flows for relevant technological applications. MHD flows in a rectangular duct have been extensively studied, but many aspects of these flows are not yet fully understood.

In this work, we analyze the effect of perpendicular magnetic field on laminar liquid lead lithium flow through a horizontal duct using 3D computational software. The combined effect of increasing the Hartmann number and buoyancy force under specific thermal boundary conditions will be discussed. We consider an insulating walls duct with rectangular cross section of height D and width 4D under a transverse magnetic field in the y-direction perpendicular to streamwise velocity of an electrically conducting liquid metal 17Li–83Pb driven by a constant pressure gradient. The main goal of this simulation is to provide the onset of MHD instability by studying the evolution of 17Li–83Pb flow for a relatively large Hartmann number range. Critical Ha_c for which the flow losses its stability is evaluated.

Problem Description and Governing Equations

We consider the steady flow of an incompressible liquid metal in a rectangular duct with insulating walls and with an externally applied magnetic field perpendicular to flow direction. The schematic of the physical and computational domains is shown in Fig. 1. The dimensions of the duct are $L = 31.5$ mm (length), $E = 12$ mm (width), and $D = 3$ mm (height). The cross section has a rectangular shape, E and D are the rectangular duct characteristics (width–height) perpendicular and parallel to the external magnetic field. x, y, and z are, respectively, the streamwise, wall normal, and spanwise coordinates.

The working fluid is 17Li–83Pb with constant density ρ, kinematic viscosity ν, and electric conductivity σ. Flow moves in the x-direction with mean velocity $V_0 = 5$ cm/s at the inlet. Fixed temperatures are imposed on the walls of the melt duct and the inlet interface; viscous dissipation and Joule heating are negligibly small. The magnetic Reynolds number, $\mathrm{Rm} = V_0 D/\eta$, is so small that the flow field does not affect the magnetic field where $\eta = 1/\sigma\varepsilon$ is the magnetic diffusivity. The magnetic permeability ε is the same everywhere and equal to the vacuum magnetic permeability ($\varepsilon = \varepsilon_0$). The physical properties of lead lithium 17Li–83Pb used in our simulations are presented versus temperature in Table 1 [26].

For an incompressible MHD flow in a duct, the MHD equation set consists of equations for conservation of mass, conservation of momentum in three directions, and the equation governing the electric potential. The magnetic field induces an electric current, which is calculated from the electric potential field. The fundamental MHD equations governing the motion of an incompressible electrically conducting liquid–metal fluid in a rectangular duct can be expressed as follows:

$$\rho\left[\frac{\partial \boldsymbol{V}}{\partial t} + (\boldsymbol{V}\cdot\nabla)\boldsymbol{V}\right] = -\nabla P + \rho\nu\nabla^2\boldsymbol{V} + \boldsymbol{j}\times\boldsymbol{B} + \boldsymbol{f} \tag{1}$$

$$\nabla\cdot\boldsymbol{V} = 0 \quad \text{and} \quad \nabla\cdot\boldsymbol{j} = 0 \tag{2}$$

$$\frac{\mathbf{J}}{\sigma} = -\nabla\varphi + \boldsymbol{V}\times\boldsymbol{B} \tag{3}$$

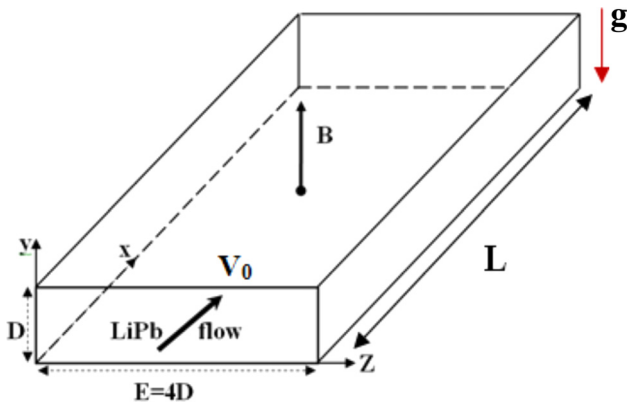

Fig. 1 Physical and computational geometry used for numerical simulations

Table 1 Physical properties of liquid metal 17Li–83Pb

Lead lithium eutectic 17Li–83Pb	
Density (kg/m^3)	$10.45\times10^{-3}(1–161\times10^{-6}T)$
Volume expansion coefficient (K^{-1})	$\beta\sim161\times10^{-6}$
Thermal conductivity (W/cm K)	$k = 1.95\times10^{-2} + 19.6\times10^{-5}T$
Specific heat (J/mol K)	$C_p = 33.77 - 1.58\times10^{-3}T$
Electrical resistivity (Ω cm)	$R = 102.3\times10^{-2} + 0.0426\times10^{-6}T$
Viscosity μ (mPa·s)	$\mu = 0.187\mathrm{e}^{11640/8.314T}$
Magnetic permeability (h/m)	1.257×10^{-6}
Melting temperature T_m (K)	508

$$\frac{\partial \mathbf{T}}{\partial t} + \boldsymbol{V} \cdot \nabla T = \frac{\boldsymbol{K}}{\rho C_p} \nabla^2 T \tag{4}$$

where V, P, J, B, φ, and t are velocity, pressure, current density, applied magnetic field, electrical potential. and time, respectively. The term $\boldsymbol{f}$ on the right-hand side of the momentum equation denotes the gravitational force. The Boussinesq approximation states that fluid density is a linear function of temperature in the gravitational body force term given as $f = \rho\beta(T - T_m)g$, where β is the thermal expansion coefficient and T_m is the melting temperature.

Typically, liquid metal MHD flow is characterized by various dimensionless parameters. The square of Hartmann number $\mathrm{Ha} = BD\sqrt{\sigma/\rho\nu}$ characterizes the ratio of electromagnetic and viscous forces. The hydrodynamic Reynolds number $\mathrm{Re} = V_0 D/\nu$ evaluates the ratio of inertial forces to viscous forces. The interaction parameter measures the ratio of electromagnetic force to inertial forces, it is given by $N = \mathrm{Ha}^2/\mathrm{Re}$. The dimensionless numbers are defined based upon the duct height (D) and the bulk mean velocity V_0. The width and aspect ratio of the duct are, respectively, $\Gamma_1 = E/D = 4$ and $\Gamma_2 = L/\mathrm{D} = 10.5$. The Prandtl number $\mathrm{Pr} = \nu/\alpha$ characterizes the importance of thermal diffusivity compared to momentum diffusivity where α is the thermal diffusivity. The contribution of buoyancy with respect to viscous forces is described by the Grashof number $\mathrm{Gr} = g\beta\Delta T D^3/\nu^2$, where g is the acceleration of gravity and ΔT is the characteristic temperature difference.

Boundary Conditions and Numerical Method

For the present computation, the velocity boundary condition at the inlet is imposed as fully developed laminar profile and at the outlet surface of duct is the outflow condition. The velocity boundary conditions are no slip at walls. Fixed temperatures are imposed on the walls, upper plate ($T_{\mathrm{Up}W} = 823\,\mathrm{K}$), and lower plate ($T_{\mathrm{Lo}W} = 623\,\mathrm{K}$). The problem is solved using the finite volume package FLUENT with a 3D double solver, the second order upwind discretization for convection, the SIMPLEC algorithm for pressure–velocity coupling, and the body force weighted scheme for pressure interpolation. For electric potential equations, the second-order upwind is used for the electrical potential gradient term. Convergence is handled by monitoring residuals of continuity, momentum, and energy equations. The value of the Prandtl number characterizing the lead lithium liquid is $\mathrm{Pr} = 0.017$. Grashof and Reynolds numbers are fixed to $\mathrm{Gr} = 10^6$ and $\mathrm{Re} = 1363$ (based upon total duct height D). In the present manuscript, we fixed the Reynolds number of 1363 corresponding to the mean velocity of Pb–17Li melt 5 cm/s based on the experimental studies in Riga where the movement of this type of flow is realized [27,28]. The computational domain is meshed with

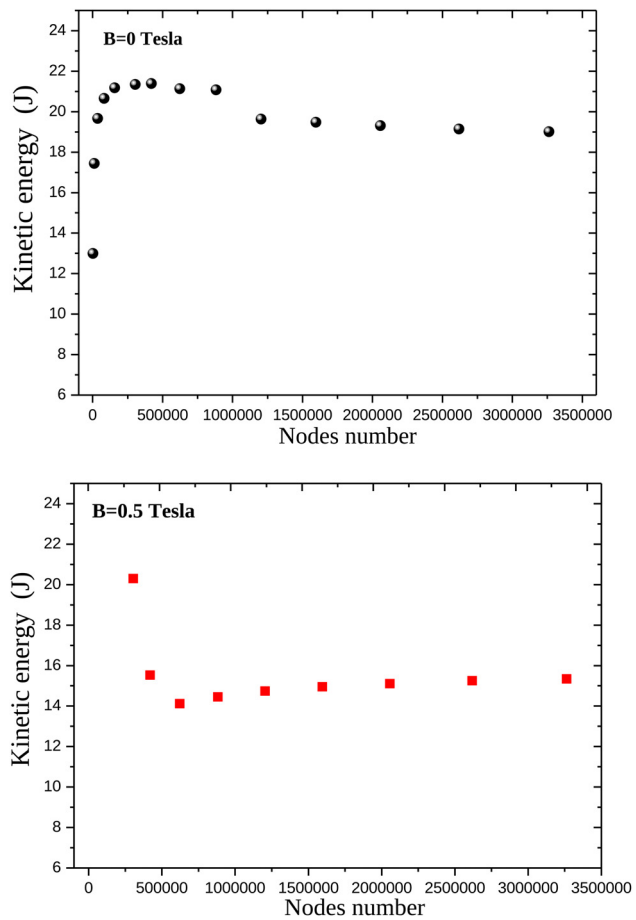

Fig. 2 Results for 3D grid dependency

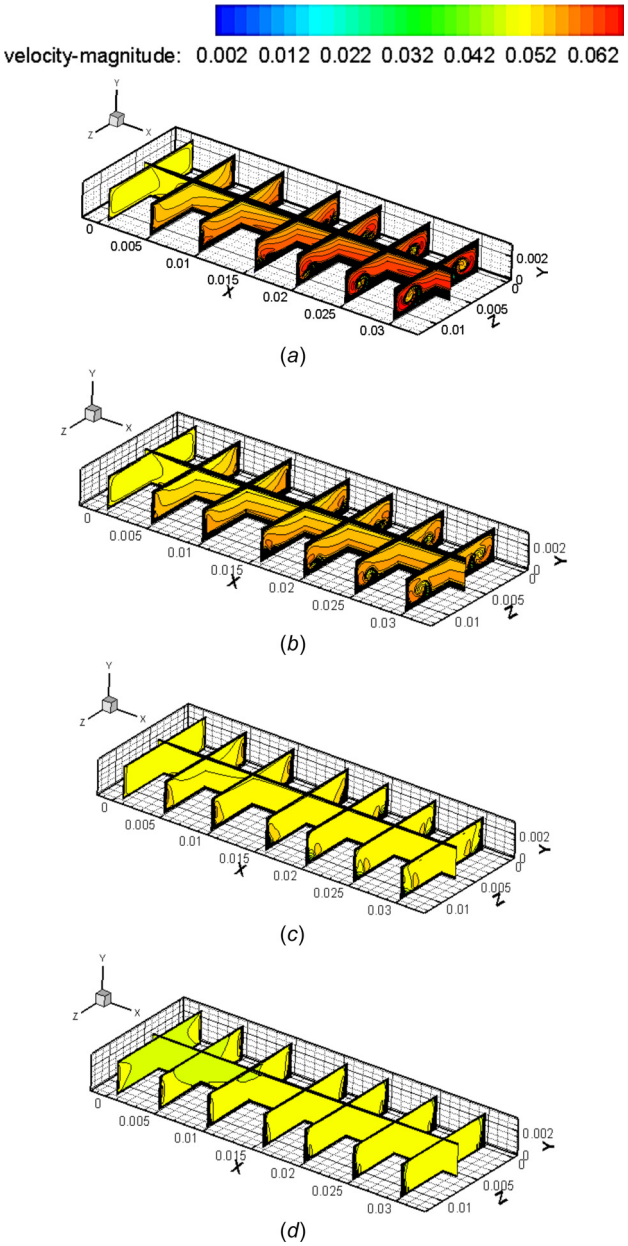

Fig. 3 Velocity distribution in different cross sections with buoyancy effect for varying Hartmann numbers Ha = 0, Ha = 16, Ha = 40, and Ha = 80

structured grid style. By carrying out the convergence test of grid with and without magnetic field for vorticity, pressure, and Nusselt number, we choose a structured grid of about 2×10^6 nodes, Fig. 2.

Results and Discussion

A 3D 17Li–83Pb flow in a rectangular cross section duct is considered with the presence of a magnetic field in the y-direction as described in Fig. 1. This flow is driven by a constant pressure gradient with mean velocity $V_0 = 5$ cm/s. The simulations are done for different Hartmann numbers with and without buoyancy effect. The MHD analysis is compared to a reference hydrodynamic case $\mathrm{Ha} = 0$. The cases of MHD flow at $\mathrm{Re} = 1363$ and $0 \leq \mathrm{Ha} \leq 120$ corresponding to the range of interaction parameter number $0 \leq N \leq 10$ are studied.

We start the discussion by analyzing the velocity distribution in the duct for different magnetic field values with and without the buoyancy effect. Figure 3 illustrates the magnetic field effect on velocity distribution taking into account the buoyancy force for different Hartmann numbers. For the hydrodynamic case ($\mathrm{Ha} = 0$), the flow structure reveals the formation of vortices pair near the side walls starting from the midlength of the duct at $x = 0.01575$ mm and they are more developed from $x = 0.025$ mm. It is clearly indicated that in this region, the velocity gradients are very large leading to the formation of thin hydrodynamic boundary layers close to the walls. The application of a vertical magnetic field dampens the flow and reduces the velocities in the core region as shown in Figs. 3(*b*)–3(*d*). The vortex structure breaks up into small structures as shown in the bottom corners for $\mathrm{Ha} = 40$ and totally disappearance for $\mathrm{Ha} = 80$.

The liquid metal flow interacts with the magnetic field by inducing an electric field $E = V \times B$. The potential difference created between the two side walls generates an electric current in the conducting fluid. The current components which are perpendicular to the magnetic field lines induce a Lorentz force $F_L = j \times B$ that acts in the bulk flow against the driving external pressure difference and tends to delay the flow and suppresses the vortices generated by the buoyancy effect especially for $\mathrm{Ha} = 80$ case. In the core region where velocity is higher, the Lorentz force exerts stronger braking while in the regions with lower velocities acts as an accelerator.

Let us now discuss the effect of thermal buoyancy by comparing Figs. 3 and 4. Two symmetric rolls are formed close to the exit of the duct when the gravity is present in the hydrodynamic case. The flow exhibits different patterns in the case without buoyancy and velocity tends to be more stable. The absence of gravity field may thus play a stabilizing role in the core region where no vortices are formed. We note that when Ha increases the thickness of parallel boundary layer increases in both cases with and without buoyancy (see $\mathrm{Ha} = 16$, $\mathrm{Ha} = 40$, and $\mathrm{Ha} = 80$). The increase in the Hartmann number leads to stronger stabilization effects; as a result, the velocity gradients are very high in the boundary layers because they become very thin while the core flow disperses out over a part of the cross section.

Figure 5 provides the contours of streamwise velocity and velocity vectors throughout the flow at three cross sections, near the inlet ($x = 0.005$ m), at the middle ($x = 0.01575$ m), and near the outlet ($x = 0.03$ m) in the cases without ($\mathrm{Ha} = 0$) and with MHD effect ($\mathrm{Ha} = 16$ and $\mathrm{Ha} = 80$). The velocity vectors are displayed in the bulk flow in order to highlight the interaction of liquid metal motion and to show the behavior direction of the fluid particle in the cross section of the duct. Through the cross sections for $\mathrm{Ha} = 0$ considering the buoyancy, the flow field evolves progressively being from the inlet to the outlet. A substantial flow development between the mid and the outlet of the duct is shown by the vectors. This flow regime gives rise to the formation of considerable instability patterns. The flow moves from the upper plate to the lower plate and the buoyant forces generate two counter rotating vortices near the side walls symmetric to the y-direction. For relatively weak Hartmann number $\mathrm{Ha} = 16$, the gradual disappearance of cells is observed and the velocity gradients near the Hartmann walls increase. For Hartmann number $\mathrm{Ha} = 80$, strong Lorentz force conducts to stabilize the core flow and increases the thickness of the side boundary layers. However, it decreases the Hartmann boundary layer thickness.

Thick boundary layers near the walls favor to promote a high interaction of liquid metal with the solid wall. In this Shercliff case, all walls are nonconducting with the presence of a vertical temperature gradient. The duct walls perpendicular to the magnetic field (upper and lower plates) are the Hartmann walls, whereas the walls parallel to the field (face a and face b) are the side walls, Fig. 5(*b*). This flow through a rectangular duct shows evidence of two types of boundary layer. The Hartman layers are the boundary layer which exhibit at the walls perpendicular to the magnetic field, whose thickness in a strong magnetic field scales as $\delta_{\mathrm{Ha}} = 1/\mathrm{Ha}$. The side layers have a thickness scaling as $\delta_{\mathrm{side}} = 1/\sqrt{\mathrm{Ha}}$ [29].

Figure 6(*a*) depicts the effect of Hartmann number in the range $0 < \mathrm{Ha} \leq 120$ on the maximum velocity of the flow in cases with and without buoyancy effect. It can be seen that the velocity varies as a parabolic function of Ha in both cases. It decreases in the range of Hartman number $0 < \mathrm{Ha} \leq 63$, while it increases for $\mathrm{Ha} > 63$. A critical magnetic field intensity $B_C = 0.8$ T corresponding to $\mathrm{Ha}_{c1} = 63$ separating two different MHD regimes is clearly observed. The presence of this critical threshold is due to the fact that the maximum velocity is located inside the bulk flow in the first range $0 < \mathrm{Ha} \leq 63$ while it corresponds to the velocity in the boundary layer in the second range $63 < \mathrm{Ha} \leq 103$. The application of magnetic field $\mathrm{Ha}_{c1} = 63$ is sufficient to the flow braking

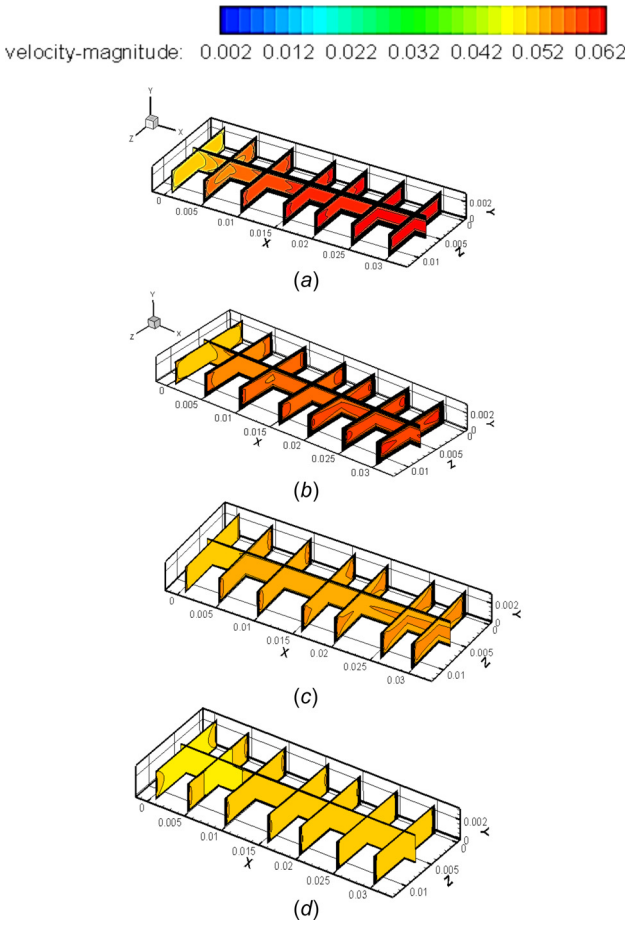

Fig. 4 Velocity distribution in different cross section without the buoyancy effect for different Hartmann numbers Ha = 0, Ha = 40, and Ha = 80

without having adverse effects on the walls of the duct and thus eliminate the fluid flow-wall interaction. Let us now discuss the buoyancy effect on the maximum velocity for different Ha values. We note that for relatively small values of Ha, $0 \leq Ha \leq 63$, the velocity values are almost the same in the cases without and with buoyancy as the obtained points are almost superposed in this range. On the contrary, the buoyancy effect is more pronounced in the range $63 < Ha \leq 120$ as the maximum velocities record a significant increase. This difference can be justified by discussing Figs. 6(*b*)–6(*e*).

Figures 6(*b*) and 6(*c*) show the velocity distribution in the Hartmann layers with thermal buoyancy when Ha varies in the range $0 \leq Ha \leq 120$. These data correspond to the middle (y, z) plane of the flow in the y-direction at $z = 0.006$ m and a Reynolds number $Re = 1363$. The hydrodynamic velocity profile ($Ha = 0$) is inclined in comparison with the magnetohydrodynamic profile and the case without buoyancy, Fig. 6(*d*). It exhibits the no symmetry to the y-direction as shown in Fig. 6. We notice that for y varying in the range $0.25 \leq y \leq 0.5$, the velocity values are larger relatively to those located in the range $0.25 \leq y \leq 0.8$. The velocity profile becomes progressively more flat and straight when Ha increases and the maximum velocity decreases in the core region and is directed toward the Hartmann walls. The core fluid velocity decreases relatively for about 7%, 13.5%, 16.7%, 17.82%, 18.83%, and 19.3%, respectively, for $Ha = 16$, $Ha = 40$, $Ha = 63$, $Ha = 80$, $Ha = 95$, and $Ha = 103$. The solid walls that confine the fluid are assumed to be insulating, the induced currents are closed within the flow domain. As the lead lithium is an electrically conducting fluid, the effect of electromagnetic braking changes drastically the flow in the core region as shown for $Ha = 40$ and $Ha = 63$ in Fig. 6(*b*). This braking effect results from the interaction of the induced electric current in flow domain with the magnetic field. The velocity increases near the Hartmann walls as shown by the M-shaped profile and creates strong jet on the walls for $Ha = 80$, $Ha = 95$, and $Ha = 103$, Fig. 6(*c*). The buoyancy acts together with the MHD force to intensify the flow near the Hartmann layers which can be demonstrated by the distance between the two curves of Fig. 6(*a*) and the higher picks of Fig. 6(*c*) with respect to Fig. 6(*e*) in the range $63 \leq Ha \leq 103$.

Figure 7 shows the plots of the axial velocity for different Ha values in order to better understand their evolution along the flow direction. When the magnetic field increases, the axial velocity

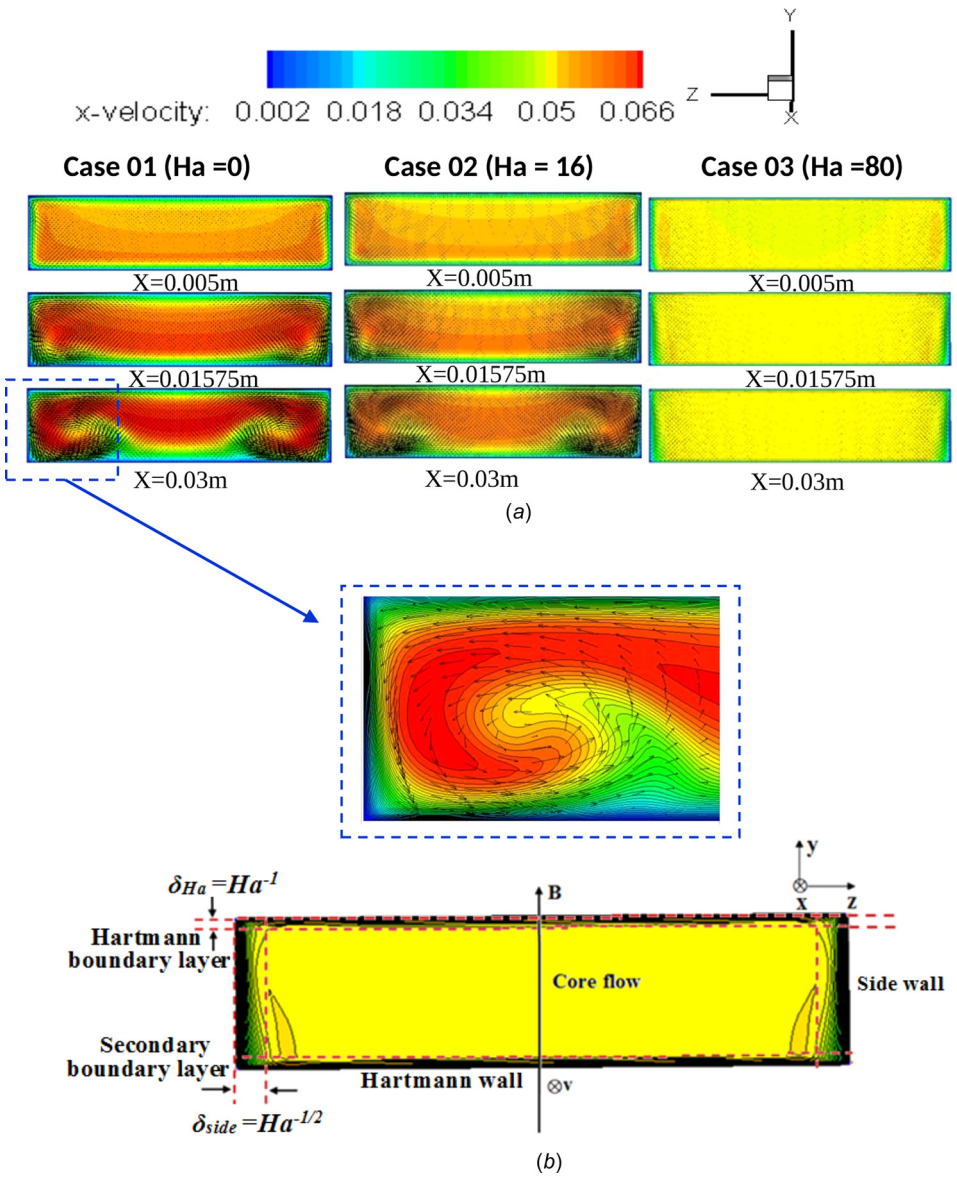

Fig. 5 (*a*) Streamwise velocity contours and secondary velocity vectors buoyancy effect in three cross sections for Ha = 0, Ha = 16, Ha = 40, and Ha = 80 and (*b*) cross-sectional area of duct with various regions of flow for Ha = 80

decreases. For the reference case (Ha = 0), the axial velocity increases exponentially to reach the maximum value at the outlet. For weak magnetic field intensities ($Ha < Ha_{C1}$), velocity gradient is strongly reduced compared to the hydrodynamic case. A specific variation is observed near the duct inlet for $Ha > Ha_{C1}$ where the velocity decreases until $x = 0.067$ as it is shown by a dashed line then it remains almost constant along the duct.

Let us now investigate the effect of magnetic field on heat transfer with and without buoyancy. We present in Fig. 8 the temperature evolution in different cross sections with and without buoyancy effect for various Hartmann number values. Temperature increases from the inlet to the outlet of the duct as depicted in Fig. 8(*a*). We have found in our previous work [8] that the magnetic field has more impact on the flow pattern than on the temperature field.

Temperature evolves from a nearly parabolic profile near the inlet to a linear profile at the outlet as shown in Fig. 8(*b*). From Figs. 8(*c*) and 8(*d*), we report that when the drag force of the fluid is increased, the temperature is increased too substantially in comparison to the case without buoyancy which exhibits flatten profile in the duct core. With increasing Hartmann number in the buoyancy case, the temperature profile increases about 1.46% in the duct core. Near the side walls, the thermal boundary layer presents a large temperature gradient.

In Fig. 9, the critical appearance of MHD instability at $Ha_{c2} = 120$ is presented. The possibility of vortex generation in duct flow under strong magnetic field can appear due to current loops in the flow direction. These streamwise currents that produce Lorentz forces in toward the side walls generate internal shear layers that can become unstable and lead to raise the corrosion rate. We note that MHD vortices created under a strong magnetic field have the tendency to align their axes in the flow direction as reported by Moreau et al. [27]. Vorticity can be created in the presence of uniform magnetic field through the

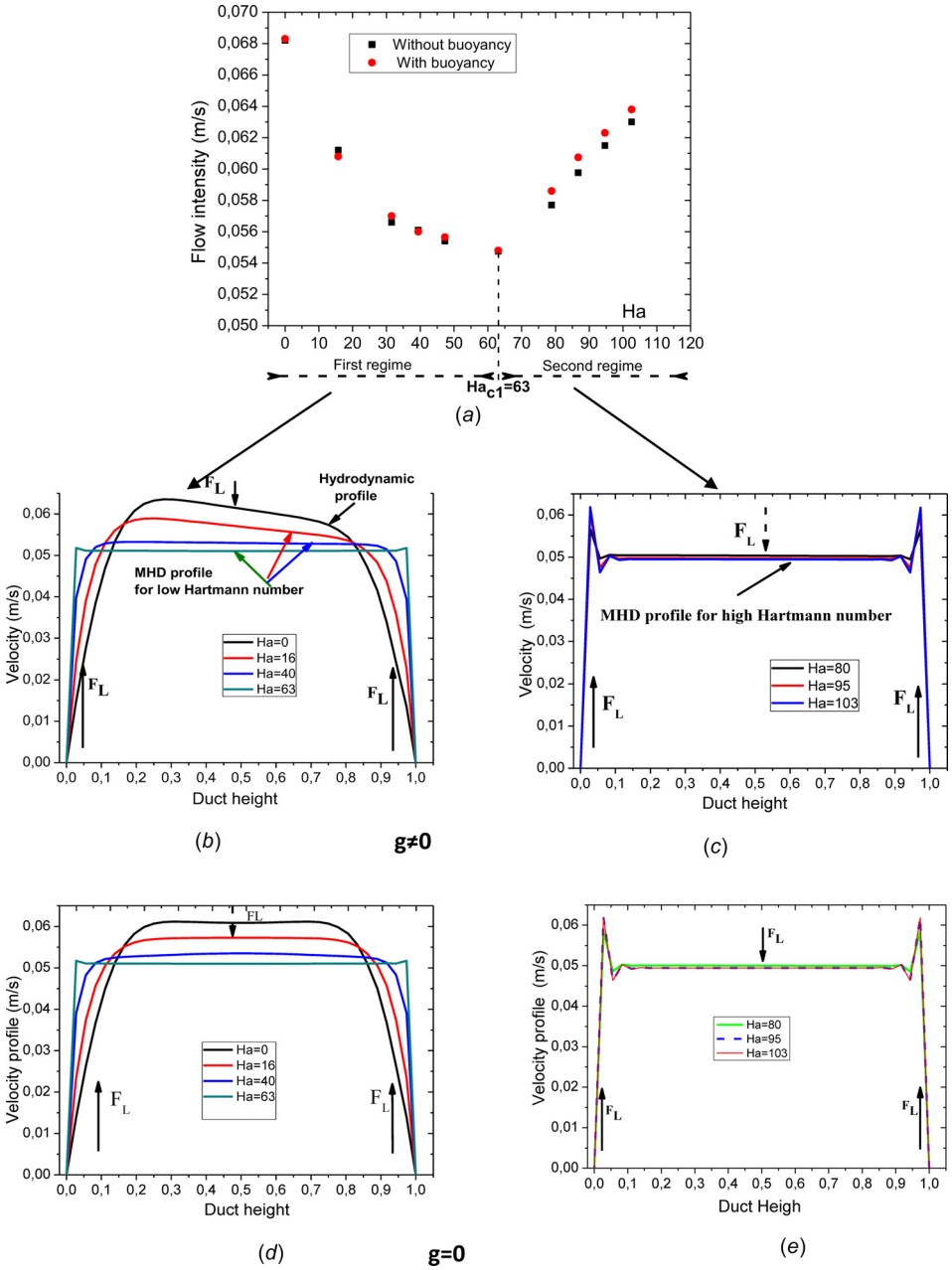

Fig. 6 Velocity distribution for different Hartmann number without and with buoyancy field: (*a*) maximum velocity, (*b*) Hartmann velocity profile with buoyancy effect at $z = 0.006$ m for weak Ha, (*c*) Hartmann velocity profile with buoyancy effect at $z = 0.006$ m for large Ha, (*d*) and (*e*) velocity profile in the Hartmann layers for laminar flow without buoyancy

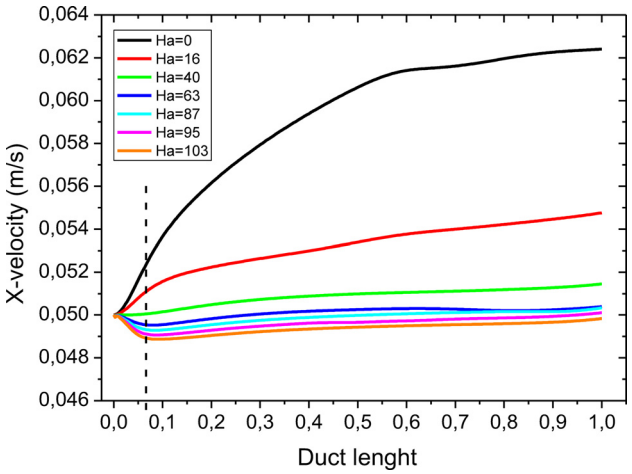

Fig. 7 X-velocity evolution along the center of the duct for different Hartmann number with buoyancy effect

buoyancy effect. It seems that many factors may affect the liquid metal flow stability near the walls. When the vertical magnetic intensity increases, the flow near the walls undergoes disturbances and eventually jets as secondary flow. The high velocity gradients in the Hartman and side layers can cause instabilities and streaks in the flow direction which increases the corrosion rate of the steel as observed and reported in Riga experiments [28,30]. We suggest that the Lorentz force acts strongly on the liquid metal flow within the boundary layer promoting then the wrenching of iron from steel walls.

Conclusion

Three-dimensional numerical simulations of 17Li83Pb MHD buoyant driven flow in a rectangular duct subjected to a transverse magnetic field without and with buoyancy are presented. The results show that the velocity profile is substantially changed through the rectangular cross section with perfectly electrically insulating walls. The structure of the velocity field is sensitive to the imposed magnetic field.

The buoyancy force creates and influences the distribution of vortices in the fluid and determines the flow pattern and its structure. The application of a vertical magnetic field dampens the flow and reduces the velocities in the core region due to flattening effects. The vortex structure breaks up into small structures and then disappears. In particular, the relatively high Hartmann number affects strongly the boundary layer region that represents a significant characteristic feature of the MHD flow. Velocity profiles demonstrate peaks near the side walls which have higher value than in the core region. Velocity gradients become very important close to the walls accelerating then the flow and increasing the skin friction. This effect could increase possibly the corrosion rate of the walls by molten metal. Strong Hartman number promotes the formation of the "M-shaped" velocity profile and exerts stronger braking in the core region where velocity is higher while in the regions with lower velocities acts as an accelerator. The increase in the Hartmann number leads to stronger

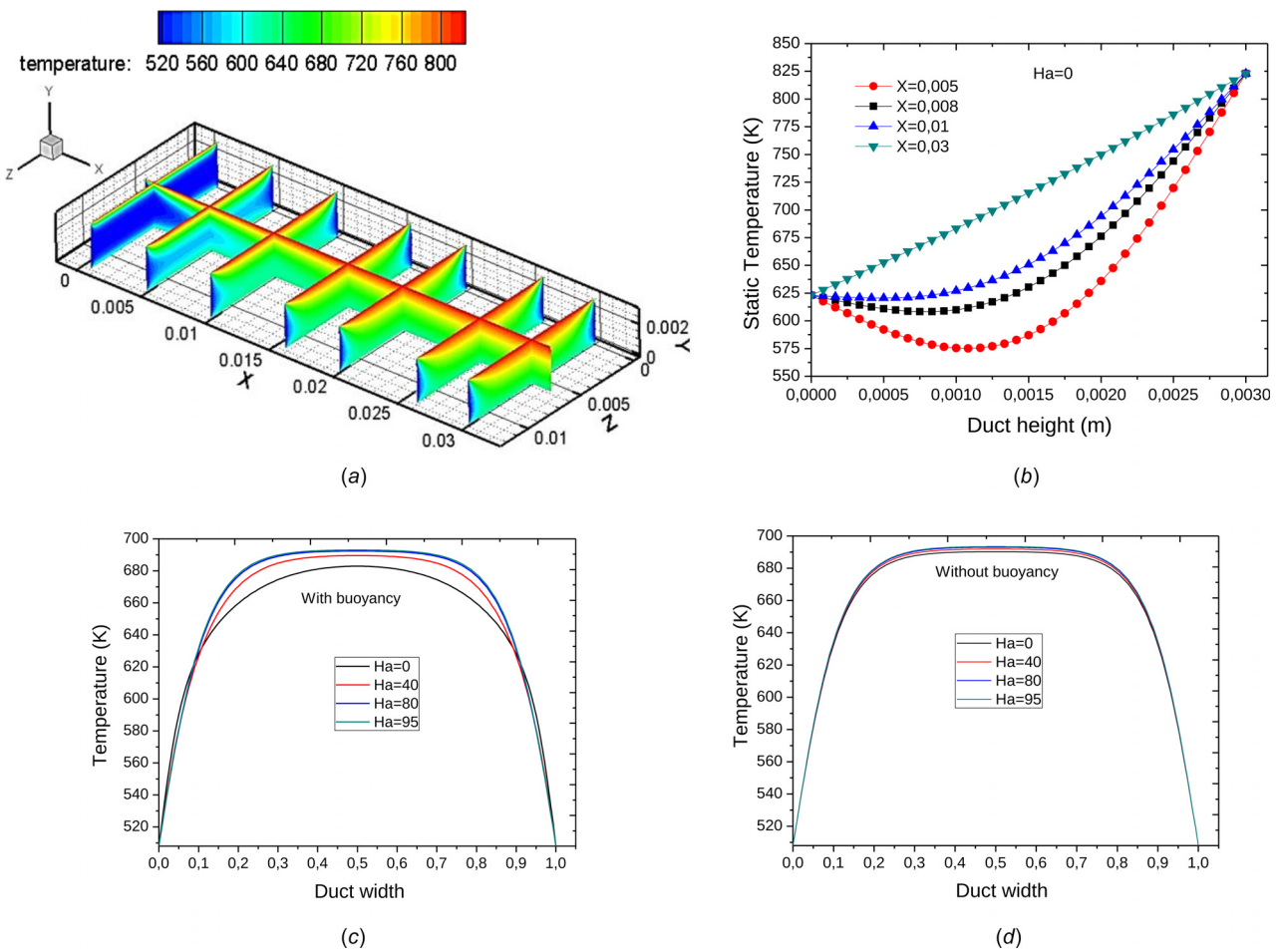

Fig. 8 Temperature distribution profile: (*a*) in different planes with buoyancy effect, (*b*) in different cross section for Ha = 0, (*c*) case with buoyancy for various Ha, and (*d*) case without buoyancy for various Ha

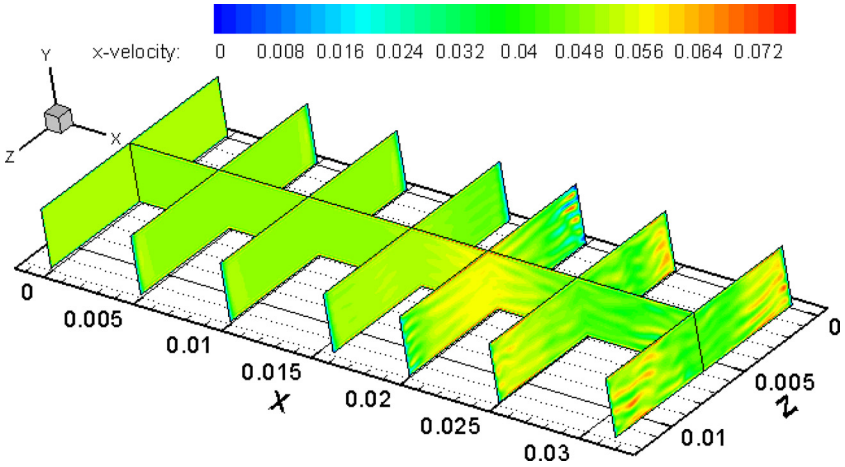

Fig. 9 Onset of MHD instability for critical Hartmann number $Ha_{c2} = 120$ with the buoyancy effect

stabilization effects. Vortices generated by the gravitational effect are suppressed for Ha = 80 case.

A critical Hartmann number $Ha_{C1} = 63$ separating two different MHD regimes is found. It is sufficient to the flow braking without having undesirable effects on the walls of the duct and thus minimizing mass transfer occurring at the walls (corrosion). The maximum velocity corresponds to the core flow in the first regime while it corresponds to the velocity in the boundary layer in the second one where the buoyancy effect is more pronounced. MHD instability is found at the Hartmann number $Ha_{c2} = 120$. Small vortices are generated near the side walls creating strong velocity gradients.

Nomenclature

C_p = specific heat (J/mol K)
D = duct height (mm)
E = duct width (mm)
Gr = Grashof number
Ha = Hartmann number
k = thermal conductivity (W/cm K)
L = duct length (mm)
N = interaction parameter number
Pr = Prandtl number
R = electrical resistivity (Ω cm)
Re = Reynolds number
Rm = magnetic Reynolds number
t = time (s)
T_m = melting temperature (K)
V_0 = velocity (cm/s)
β = volume expansion coefficient (K^{-1})
Γ = aspect ratio
δ_{Ha} = thickness of Hartman layer
δ_{side} = thickness of side layer
ε = magnetic permeability (h/m)
ε_0 = vacuum magnetic permeability (h/m)
η = magnetic diffusivity (m^2/s)
ν = kinematic viscosity (m^2/s)
ρ = density (kg/m^3)

References

[1] Gupta, A. K., Beeŕ, J. M., Louis, J. F., Busnaina, A. A., and Lilley, D. G., 1982, "Flow Aerodynamics Modeling of an MHD Swirl Combustor: Calculations and Experimental Verification," ASME J. Fluids Eng., **104**(3), pp. 385–391.

[2] Mokhtari, F., Bouabdallah, A., Merah, A., and Oualli, H., 2012, "Numerical Investigation of Magnetic Field Effect on Pressure in Cylindrical and Hemispherical Silicon CZ Crystal Growth," Cryst. Res. Technol., **47**(12), pp. 1269–1278.

[3] Smolentsev, S., Vetcha, N., and Abdou, M., 2013, "Effect of a Magnetic Field on Stability and Transitions in Liquid Breeder Flows in a Blanket," Fusion Eng. Des., **88**(6–8), pp. 607–610.

[4] Kharicha, A., Teplyakov, I., Ivochkin, Y., Wu, M., Ludwig, A., and Guseva, A., 2015, "Experimental and Numerical Analysis of Free Surface Deformation in an Electrically Driven Flow," Exp. Therm. Fluid Sci., **62**, pp. 192–201.

[5] Jin, K., Vanka, S. P., and Thomas, B. G., 2015, "Three-Dimensional Flow in a Driven Cavity Subjected to an External Magnetic Field," ASME J. Fluids Eng., **137**(7), p. 071104.

[6] Kumamaru, H., and Fujiwara, Y., 1998, "Pressure Drop and Heat Transfer of Magnetohydrodynamic Annular Two-Phase Flow in Rectangular Channel," ASME J. Fluids Eng., **120**(1), pp. 152–159.

[7] Hunt, J. C. R., 1965, "Magnetohydrodynamic Flow in Rectangular Ducts," J. Fluid Mech., **21**(04), pp. 577–590.

[8] Tigrine, Z., Mokhtari, F., and Bouabdallah, A., 2015, "3D Computational Investigation of Vertical Magnetic Field Effect on Heat Transfer and 83Pb–17Li Flow," Magnetohydrodynamics, **51**(1), pp. 83–94.

[9] Dholey, S., 2014, "Effect of Radial Temperature Gradient on the Stability of Magnetohydrodynamic Dean Flow in an Annular Channel at High Magnetic Parameter," ASME J. Fluids Eng., **137**(3), p. 031203.

[10] Rashidi, S., Bovand, M., Esfahani, J. A., Öztop, H. F., and Masoodi, R., 2015, "Control of Wake Structure Behind a Square Cylinder by Magnetohydrodynamics," ASME J. Fluids Eng., **137**(6), p. 061102.

[11] Midya, C., Layek, G. C., Gupta, A. S., and Ray Mahapatra, T., 2004, "Magnetohydrodynamic Viscous Flow Separation in a Channel With Constrictions," ASME J. Fluids Eng., **125**(6), pp. 952–962.

[12] Eckert, E. R. G., and Irvine, T. F., Jr., 1960, "Pressure Drop and Heat Transfer in a Duct With Triangular Cross Section," ASME J. Heat Transfer, **82**(2), pp. 125–136.

[13] Daschiel, G., Frohnapfel, B., and Jovanovic, J., 2013, "Numerical Investigation of Flow Through a Triangular Duct: The Coexistence of Laminar and Turbulent Flow," Int. J. Heat Fluid Flow, **41**, pp. 27–33.

[14] Walker, J. S., 1987, "Liquid Metal MHD Flow in a Duct Whose Cross Section Changes From a Rectangle to a Trapezoid," Int. J. Eng. Sci., **25**(3), pp. 351–371.

[15] Hunt, J. C. R., and Leibovich, S., 1967, "Magnetohydrodynamic Flow in Channels of Variable Cross-Section With Strong Transverse Magnetic Fields," J. Fluid Mech., **28**(02), pp. 241–260.

[16] Hartmann, J., 1937, *Mercury Dynamics I. Theory of the Laminar Flow of an Electrically Conductive Liquid in a Homogeneous Magnetic Field* (Matematisk-Fysiske Meddelelser), Det Kgl danske Videnskabernes, Germany, pp. 151–28.

[17] Shercliff, J. A., 1956, "The Flow of Conducting Fluids in Circular Pipes Under Transverse Magnetic Fields," J. Fluid Mech., **1**(06), pp. 644–666.

[18] Hunt, J. C. R., 1965, "Magnetohydrodynamic Flow in Rectangular Ducts," J. Fluid Mech., **21**(4), pp. 577–590.

[19] Hunt, J. C. R., and Stewartson, K., 1965, "Magnetohydrodynamic Flow in Rectangular Ducts," J. Fluid Mech., **23**(3), pp. 563–581.

[20] Shebalin, J. V., 2013, "Temperature and Entropy in Ideal Magnetohydrodynamic Turbulence," ASME J. Fluids Eng., **136**(6), p. 060901.

[21] Doss, E., Geyer, H., Ahluwalia, R. K., and Im, K., 1981, "Two-Dimensional Performance Analysis and Design of MHD Channels," ASME J. Fluids Eng., **103**(2), pp. 307–314.

[22] Recebli, Z., Selimli, S., and Gedik, E., 2013, "Three Dimensional Numerical Analysis of Magnetic Field Effect on Convective Heat Transfer During the MHD Steady State Laminar Flow of Liquid Lithium in a Cylindrical Pipe," Comput. Fluids, **88**, pp. 410–417.

[23] Smolentsev, S., Vetcha, N., and Abdou, M., 2013, "Effect of a Magnetic Field on Stability and Transitions in Liquid Breeder Flows in a Blanket," Fusion Eng. Des., **88**(6–8), pp. 607–610.

[24] Chutia, M., and Deka, P. N., 2015, "Numerical Study on MHD Mixed Convection Flow in a Vertical Insulated Square Duct With Strong Transverse Magnetic Field," J. Appl. Fluid Mech., **8**, pp. 473–481.
[25] Bluck, M. J., and Wolfendale, M. J., 2015, "An Analytical Solution to Electromagnetically Coupled Duct Flow in MHD," J. Fluid Mech., **771**, pp. 595–623.
[26] Jauch, U., Karcher, V., Schulz, B., and Haase, G., 1986, "Thermophysical Properties in the System Li-Pb," Kernforschungszentrum, Stuttgart, Germany, Technical Report No. SWB-057695733 (in German).
[27] Moreau, R., Brechet, Y., and Maniguet, L., 2011, "Eurofer Corrosion by the Flow of the Eutectic Alloy Pb–Li in the Presence of a Strong Magnetic Field," Fusion Eng. Des., **86**(1), pp. 106–120.
[28] Bucenieks, I., Krishbergs, R., Platacis, E., Lipsbergs, G., Shishko, A., Zik, A., and Muktep Avela, F., 2006, "Investigation of Corrosion Phenomena in Eurofer Steel in Pb–17Li Stationary Flow Exposed to a Magnetic Field," Magnetohydrodynamics, **42**(2–3), pp. 237–251.
[29] Thess, A., Krasnov, D., Boeck, T., Zienicke, E., Zikanov, O., Moresco, P., and Alboussière, T., 2007, "Transition to Turbulence in the Hartmann Boundary Layer," GAMM-Mitt., **30**(1), pp. 125–132.
[30] Platacis, E., Ziks, A., Poznjak, A., Muktepavela, F., Shisko, A., Sarada, S., Chakraborty, P., Sanjay, K., Vrushank, M., Fotedar, R., Rajendra, E. K., and Suri, A. K., 2012, "Investigation of the Li–Pb Flow Corrosion Attack on the Surface of P91 Steel in the Presence of Magnetic Field," Magnetohydrodynamics, **48**(2), pp. 343–350.